Opto-Electronic Advances

ISSN 2096-4579 CN 51-1781/TN

Exceptional-point-enhanced sensing in an all-fiber bending sensor

Zheng Li, Jingxu Chen, Lingzhi Li, Jiejun Zhang and Jianping Yao

Citation: Li Z, Chen JX, Li LZ, et al. Exceptional-point-enhanced sensing in an all-fiber bending sensor. *Opto-Electron Adv* **6**, 230019(2023).

https://doi.org/10.29026/oea.2023.230019

Received: 8 February 2023; Accepted: 25 June 2023; Published online: 21 September 2023

Opto-Electronic Advances

Article

December 2023, Vol. 6, No. 12

DOI: 10.29026/oea.2023.230019

Exceptional-point-enhanced sensing in an all-fiber bending sensor

Zheng Li[1], Jingxu Chen[1], Lingzhi Li[1], Jiejun Zhang[1]* and Jianping Yao[1,2]*

An exceptional-point (EP) enhanced fiber-optic bending sensor is reported. The sensor is implemented based on parity-time (PT)-symmetry using two coupled Fabry-Perot (FP) resonators consisting of three cascaded fiber Bragg gratings (FBGs) inscribed in an erbium-ytterbium co-doped fiber (EYDF). The EP is achieved by controlling the pumping power to manipulate the gain and loss of the gain and loss FP resonators. Once a bending force is applied to the gain FP resonator to make the operation of the system away from its EP, frequency splitting occurs, and the frequency spacing is a nonlinear function of the bending curvature, with an increased slope near the EP. Thus, by measuring the frequency spacing, the bending information is measured with increased sensitivity. To achieve high-speed and high-resolution interrogation, the optical spectral response of the sensor is converted to the microwave domain by implementing a dual-passband microwave-photonic filter (MPF), with the spacing between the two passbands equal to that of the frequency splitting. The proposed sensor is evaluated experimentally. A curvature sensing range from 0.28 to 2.74 m^{-1} is achieved with an accuracy of 7.56×10^{-4} m^{-1} and a sensitivity of 1.32 GHz/m^{-1}, which is more than 4 times higher than those reported previously.

Keywords: exceptional-point; enhanced sensitivity; bending sensor; parity-time symmetry.

Li Z, Chen JX, Li LZ, Zhang JJ, Yao JP. Exceptional-point-enhanced sensing in an all-fiber bending sensor. *Opto-Electron Adv* **6**, 230019 (2023).

Introduction

Fiber-optic sensors have been widely used for monitoring various physical and chemical quantities thanks to the advantages such as high resistance to corrosion, immunity to electromagnetic interference (EMI), and remote sensing ability[1,2]. Of many types of fiber-optic sensors, bending sensors are of particular interest for their applications including structural health monitoring, soft robotic configurations, and intelligent artificial limbs[3]. Various fiber-optic bending sensors based on a fiber Bragg grating (FBG)[4], a multi-core fiber (MCF)[5], a long-period fiber grating (LPFG)[6], or a Mach-Zehnder interferometer (MZI)[7] have been proposed. In general, the wavelength shift of a bending sensor has a linear relationship with an external bending force, making a bending sensor have limited sensitivity. To have a higher sensitivity, an effective solution is to implement a sensor to make the wavelength shift have a nonlinear relationship with an external bending force, in which a large slope results, corresponding to an increased sensitivity.

In recent years, there has been a growing interest in studying a non-Hermitian system that is operating around the exceptional point (EP), to find a new way of enhancing the sensitivity beyond what is possible in a

[1]Guangdong Provincial Key Laboratory of Optical Fiber Sensing and Communications, Institute of Photonics Technology, Jinan University, Guangzhou 510632, China; [2]Microwave Photonics Research Laboratory, School of Electrical Engineering and Computer Science, University of Ottawa, Ottawa, ON K1N 6N5, Canada.

*Correspondence: JJ Zhang, E-mail: zhangjiejun@jnu.edu.cn; JP Yao, E-mail: jpyao@uottawa.ca

Received: 8 February 2023; Accepted: 25 June 2023; Published online: 21 September 2023

conventional system[8–14]. For a non-Hermitian system operating at the EP, all eigenvalues and the corresponding eigenvectors coalesce. However, an environmental perturbation would cause the eigenvalues to split. For a small perturbation, the eigenvalue splitting at the EP is significantly large, which would provide an effective solution to measure the perturbation with significantly enhanced sensitivity through measuring the eigenvalues or frequency splitting. Such an approach in enhancing the sensing sensitivity at an EP in a whispering-galley-mode (WGM) micro-toroid cavity for nanoparticle sensing has been experimentally demonstrated[9]. In various non-Hermitian photonic systems, parity-time (PT) symmetric systems are of great interest due to the ease in manipulating the gain and loss coefficients of the coupled subsystems as well as their coupling coefficient, providing an excellent platform to explore the physics of EP[10,15–19]. For example, enhanced sensitivity was experimentally demonstrated for a PT-symmetric ternary micro-ring laser system operating at the EP[10]. The approaches reported in ref.[9,10] were implemented based on photonic integrated chips which have a key feature of small size, but may not be used for remote strain or bending sensing due to their physical structure. For remote strain or bending sensing, fiber-optic sensors may be used. Recently, fiber-optic sensors based on a nonreciprocal fiber ring cavity operating at the EP for temperature[20] and displacement[21] sensing have been proposed. Again, due to their physical structures, the sensors in ref.[20,21] cannot be employed for bending sensing.

The eigenfrequency splitting of a PT-symmetric system near its EP is usually less than a few GHz. Hence, a MHz-resolution spectrum analyzer is usually needed. A conventional optical spectrum analyzer (OSA) with a resolution of hundreds of MHz may not be able to fulfill this task. Fiber-optic sensors interrogated based on microwave photonic (MWP) techniques have recently been extensively studied[22–24]. By converting the spectral information such as wavelength shift in the optical domain to a microwave frequency change in the microwave domain, high-speed and high-resolution measurement can be achieved. A microwave photonic filter (MPF) based on phase modulation (PM) and phase-modulation to intensity-modulation (PM-IM) conversion can be implemented to convert the spectral response of an optical sensor, such as a phase-shifted FBG (PS-FBG)[22] or a micro-disk resonator (MDR)[24], to the microwave domain. By measuring the frequency response of the MPF, an increased interrogation resolution of sub kHz can be achieved thanks to the high resolution of an electric spectrum analyzer (ESA), making the microwave photonic interrogation technique a great candidate for high-resolution sensing, such as a sensor operating near its EP.

By combining the unique features of high sensitivity of a PT-symmetric sensor operating near the EP point and high resolution of microwave photonics interrogation, we propose a fiber-optic exceptional-point (EP) enhanced bending sensor based on microwave photonics interrogation with significantly increased sensing sensitivity. The sensor consists of a pair of coupled Fabry-Perot (FP) resonators implemented by inscribing three cascaded FBGs in an erbium-ytterbium co-doped fiber (EYDF). The gain and loss of the FP resonators are manipulated by controlling the pumping power to make the system operate at the EP. When a bending force is applied to the sensor through the gain resonator, mode splitting occurs. The wavelength spacing between the two splitting modes is a function of the applied bending force. Thus, by monitoring the wavelength spacing, the bending force is measured. However, direct measurement of the wavelength spacing in the optical domain is difficult considering the limited resolution of an OSA. On the other hand, if the wavelength spacing is converted to a frequency spacing in the microwave domain, a high-resolution measurement can be made by using an ESA. To do so, a dual passband MPF with the two center frequencies of the two passbands corresponding to the wavelengths of the two splitting modes is implemented, which is done based on PM and PM-IM conversion. By monitoring the spectral response of the MPF, sensing information is obtained. The proposed sensor is studied theoretically and evaluated experimentally. A mathematical expression is developed through which we can see that the wavelength spacing due to mode splitting has a square-root dependence on the applied bending force. Compared with a linear dependence, the square-root dependence makes the sensing sensitivity significantly increased. Then, the sensor is fabricated, and the performance is evaluated experimentally. The experimental results confirm the square-root dependence. For a curvature sensing range from 0.28 to 2.74 m^{-1}, a sensitivity of 1.32 GHz/m^{-1} is achieved, which is more than 4 times higher than those reported previously.

Principle

Figure 1(a) illustrates the configuration of the proposed

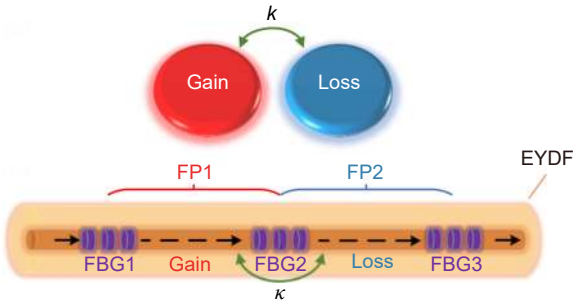

Fig. 1 | Configuration of the proposed fiber-optic sensor that consists of two mutually coupled and geometrically identical FP resonators, with one experiencing a gain and the other an equal amount of loss. The two FP resonators (FP1 and FP2) are implemented based on three uniform FBGs (FBG1, FBG2 and FBG3). FBG, fiber Bragg grating; EYDF, erbium-ytterbium co-doped fiber. The black arrow denotes the pump propagation direction.

fiber-optic sensor that consists of two mutually coupled and geometrically identical FP resonators, with one experiencing a gain and the other an equal amount of loss[25]. The two FP resonators (FP1 and FP2) are implemented based on three uniform FBGs (FBG1, FBG2 and FBG3) which are inscribed in a short and highly doped EYDF. The FP resonators are geometrically identical (FBG1 and FBG3 are identical, the lengths of FP1 and FP2 are the same, and FBG2 is a symmetric FBG) and are mutually coupled due to partial transmission/reflection of FBG2, which ensures the degeneracy of the localized resonance frequencies. A 980-nm pump light is launched into the device from the FP1 side, resulting in a higher pump power in FP1 than that in FP2 due to the absorption along the EYDF. By controlling the pump power, the gain and loss coefficients of FP1 and FP2 can be controlled to be identical in magnitude. In addition, the two FP resonators exchange energy with a coupling coefficient κ, which is determined by the transmission coefficient of FBG2. Mathematically, the modes in the system are governed by the coupled mode equations, given by[10]

$$\mathrm{i}\frac{\mathrm{d}}{\mathrm{d}t}\begin{pmatrix} a \\ b \end{pmatrix} = \begin{pmatrix} \omega_0 + \mathrm{i}g + \varepsilon & \kappa \\ \kappa & \omega_0 + \mathrm{i}\gamma \end{pmatrix}\begin{pmatrix} a \\ b \end{pmatrix}, \quad (1)$$

where g and γ are the gain and loss coefficients of FP1 and FP2, respectively, ω_0 is the localized eigenfrequency of FP1 or FP2, a and b are the electric fields of the light waves in FP1 and FP2, respectively, ε is the resonance frequency detuning between FP1 and FP2 which is proportional to the strength of the curvature perturbation $\Delta C \propto \varepsilon$ applied to FP1 without EP. Due to the wavelength-dependent reflectivity of an FBG, the gain and loss coefficients g, γ and the coupling coefficient κ are also wavelength dependent. The spectral response of the two FP resonators can be calculated by the transfer matrix method[17]. Here, only the eigenmode within the reflection bands of the three FBGs is considered. Wavelength dependence of g, γ and κ is ignored for simplicity.

We let $g = -\gamma$ to ensure PT-symmetric operation of the device. The eigenfrequencies ω_n of the supermodes in the PT-symmetric FP resonators can be calculated by

$$\omega_n = \omega_0 + \frac{1}{2}\varepsilon \pm \frac{1}{2}\sqrt{-\varepsilon^2 - 4\gamma^2 + 4\kappa^2 - 4\mathrm{i}\varepsilon\gamma}\,. \quad (2)$$

In the absence of a perturbation ($\varepsilon = 0$), Eq. (2) indicates that, when the gain/loss coefficient is having the same magnitude as the coupling coefficient (in this case, $-\gamma = \kappa$), the eigenfrequencies coalesce at $\omega_n = \omega_0$ and the system operates at its EP.

If a bending force is applied to FP1, eigenfrequency splitting would occur, and the wavelength spacing between the two split modes can be expressed as

$$\Delta\omega_{\mathrm{EP}} = \mathrm{Re}\,(\omega_1 - \omega_2) = \mathrm{Re}\left(\sqrt{-\varepsilon^2 - 4\mathrm{i}\varepsilon\gamma}\right). \quad (3)$$

If the resonance frequency detuning caused by bending is sufficiently small ($|\varepsilon| \ll |\gamma|$), Eq. (3) can be simplified as

$$\Delta\omega_{\mathrm{EP}} = \mathrm{Re}\left(\sqrt{-4\mathrm{i}\varepsilon\gamma}\right). \quad (4)$$

In our study, the sensitivity enhancement of the sensor is quantified by the enhancement factor, which is defined as the ratio between the two split modes with EP and without EP and is given by

$$\eta = \left|\frac{\Delta\omega_{\mathrm{EP}}}{\varepsilon}\right| = \left|\mathrm{Re}\left(\sqrt{\frac{-4\mathrm{i}\gamma}{\varepsilon}}\right)\right|. \quad (5)$$

As can be seen, the sensitivity enhancement is inversely proportional to the square root of the resonance frequency detuning ε, indicating that a large enhancement factor can be obtained near the EP. The calculated frequency difference between two eigenfrequencies of an EP sensor is given in Fig. 2(a) as a function of ε, which demonstrates the sensitivity is drastically enhanced as the system approaches the EP region. The slope of the response is 1/2 in the logarithmic scale, as shown in Fig. 2(b), which confirms that perturbations around the EP of a system with two eigenvalues is in the form $\Delta C^{1/2}$, which can be significantly enhanced for small values of ΔC. Figure. 2(c) shows the relationship between the perturbation and the enhancement factor, and the inset is a zoom-in view with a perturbation from 0.02 to 1

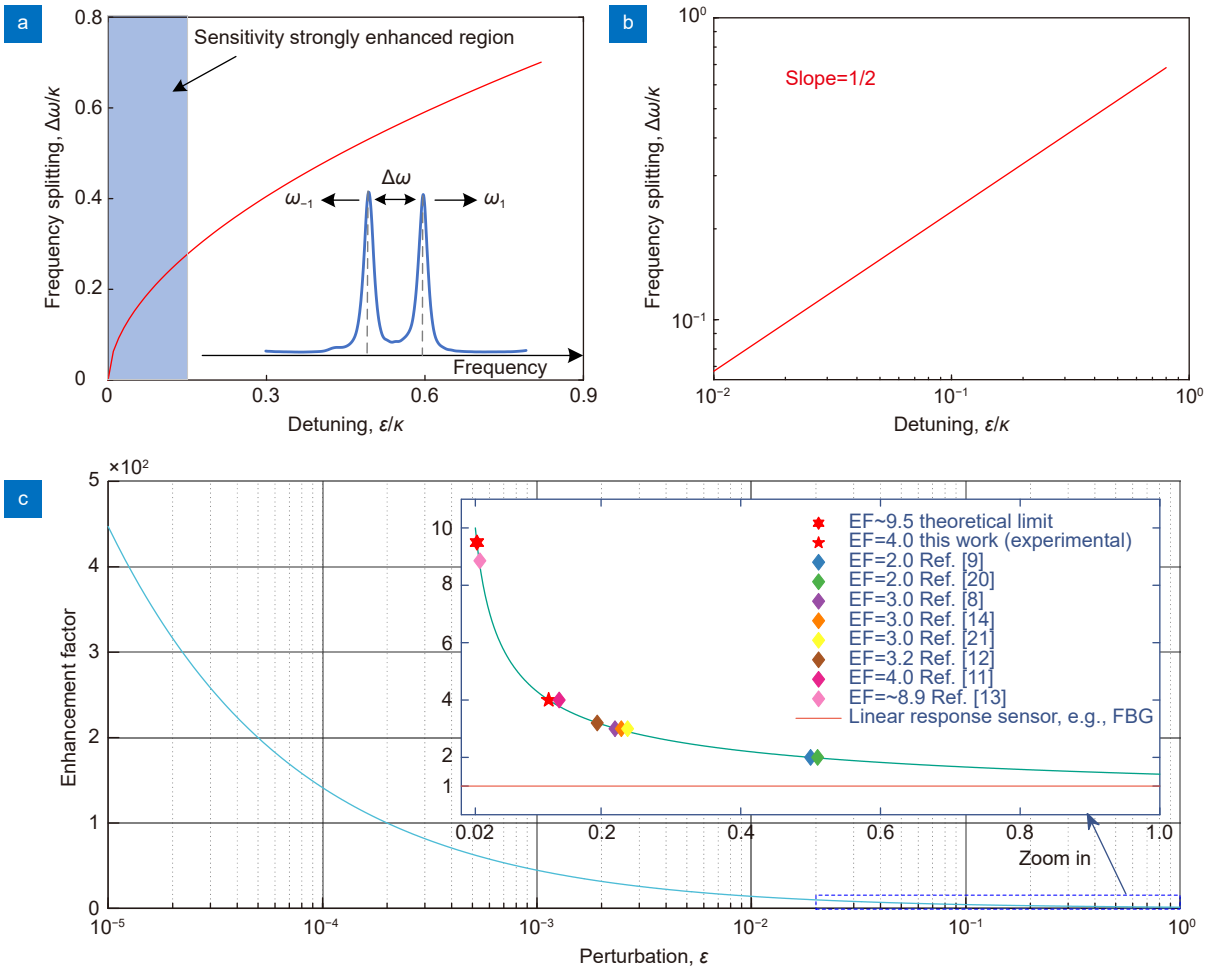

Fig. 2 | (**a**) Numerical results for the relationship between eigenfrequency splitting and resonance detuning induced by bending. (**b**) The results from (a) in a logarithmic scale. (**c**) The relationship between the sensitivity enhancement factor and perturbation. The inset is a zoom-in view, in which the enhancement factors of this work and other EP sensors are noted. The orange line represents a sensor with a linear relationship such as a conventional FBG sensor. EF: enhancement factor.

(dash-line box). As can be seen, when the perturbation is small, the enhancement factor is very large. Theoretically, when the perturbation is infinitesimal, the enhancement factor will tend to infinity. In practice, however, the smallest wavelength splitting that can be measured is limited by the bandwidths of the FP resonators. Thus, higher *Q* resonators are needed to achieve higher sensitivity and resolution. In Fig. 2(c), the EP-based sensitivity enhancement factors of some recent works using photonic integrated devices are shown. Thanks to the all-fiber implementation, the PT-symmetric FP resonators have higher *Q* factors, and the sensor would have a higher sensitivity and resolution. As a comparison, the sensitivity of a conventional fiber-optic sensor with a linear relationship, such as an FBG-based sensor, is also shown in the inset of Fig. 2(c). In the case of small perturbations, the sensitivity gap between a conventional sensor and an EP-based sensor is very large, showing the superiority of an EP sensor for sensing, especially for weak perturbation monitoring.

Results and discussion

An experiment is performed based on the experimental setup shown in Fig. 3. The device was fabricated by inscribing three FBGs to form two FP resonators in an EYDF (EY305 from CorActive) using a phase mask which was illuminated by the light from a 193-nm ArF excimer laser. The reflectivity and bandwidth of each of the three FBGs are 94% and 0.2 nm. The device has a total length of 32 mm. The distance between adjacent gratings was controllable by laterally moving the phase mask during the inscription process. In the experiment, FBG2 and FBG3 are fixed on two micro-positioning platforms (MPP2 and MPP3) and a short section of fiber

pigtail connected to FBG1 is fixed on a third MPP (MPP1) such that the curvature of FP1 can be varied. The fiber bending operation is achieved through moving MPP1 in the horizontal direction, to introduce a curvature perturbation to the resonator with a gain (FP1). The curvature is given by[26]

$$C = \frac{1}{R} = \sqrt{\frac{24x}{(L_0 - x)^3}}\,, \tag{6}$$

where L_0 is the initial distance between MPP1 and MPP2, R is the radius of the curvature, and x is the feed displacement. In our case, the initial distance is 8 cm and the step displacement is 10 μm.

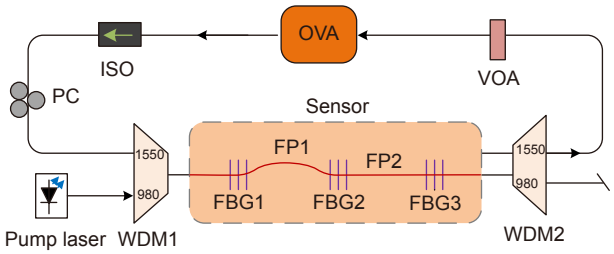

Fig. 3 | Schematic diagram of the experimental setup. OVA, optical vector analyzer; ISO, isolator; VOA, variable optical attenuator; FBG, fiber Bragg grating. PC, polarization controller; WDM, wavelength division multiplexer.

First, the spectral response of the sensor is measured. To do so, a wavelength-sweeping probe light generated by an optical vector analyzer (OVA) is applied to the sensor, as shown in Fig. 3. A 980-nm pump laser is used to pump the EYDF through the 980-nm port of a wavelength division multiplexer (WDM1), and the residual pump light is terminated at a terminator connected to the 980-nm port of WDM2. An isolator (ISO) and a variable optical attenuator (VOA) are used to avoid high-power damage to the OVA. The probe light goes through a polarization controller (PC) and is launched into the sensor through the 1550-nm port of WDM1. After passing through FP1 and FP2, the probe light is detected at the OVA through the 1550-nm port of WDM2. To achieve PT symmetry, the gain coefficient in FP1 and the loss coefficient in FP2 should be controlled identically, which are 8.75 dB and 8.47 dB by controlling the pumping power. The cavity length of FP2 can be finely tuned by adjusting the distance between MPP2 and MPP3 to ensure that FP1 and FP2 have an identical localized eigenfrequency. Both of these procedures are necessary to bring the coupled FP resonators into the EP regime.

The transmission spectrum of the sensor operating in such a state is shown in Fig. 4(a). Within the reflection bandwidth of the FBGs, the two coupled FP resonators support four resonance modes and only a single resonance peak at each resonant mode is observed. For convenience, in the experiment, we choose the marked resonance mode as the sensing mode. By moving MPP1 in the horizon direction, a curvature perturbation is applied to FP1[26]. As a result, the eigenfrequency begins to bifurcate and a frequency splitting is observed in the transmission spectrum, as shown in Fig. 4(b).

Since the spacing between the split modes is very small, it cannot be precisely measured using an OSA. We propose to interrogate the sensor by translating the wavelength spitting in the optical domain to a microwave frequency separation in the microwave domain by implementing a dual passband MPF with the center frequencies of the two passbands corresponding to the two wavelengths. The interrogation system is shown in Fig. 5. As can be seen, a CW light wave from a tunable laser source (TLS) is applied to a phase modulator via a

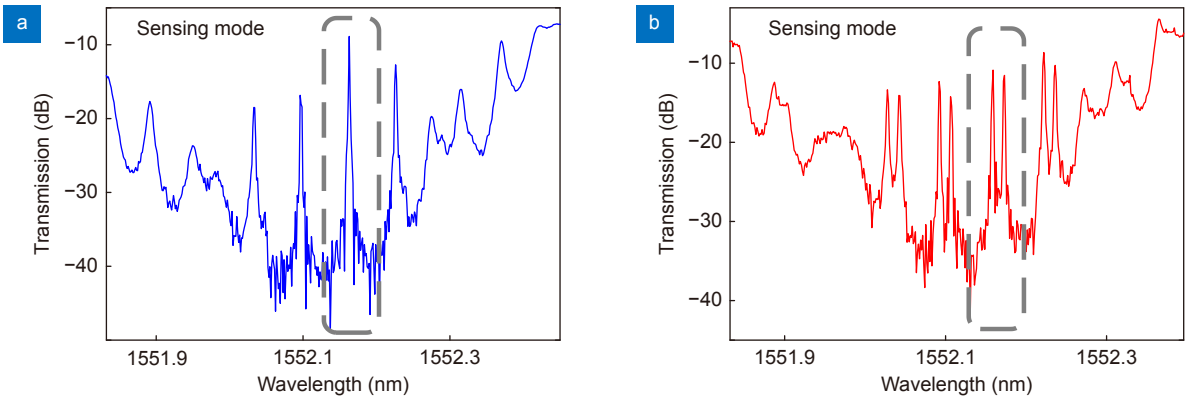

Fig. 4 | Measured transmission spectra of the sensor operating at the EP (**a**) without perturbation and (**b**) with perturbation. The sensing mode to be monitored is indicated in the dashed box.

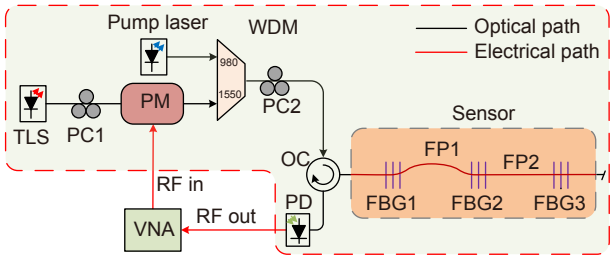

Fig. 5 | Interrogation of the sensor by translating the wavelength splitting in the optical domain to a microwave frequency separation in the microwave domain. FBG, fiber Bragg grating; TLS, tunable laser source; PC, polarization controller; PM, phase modulator; WDM, wavelength division multiplexer; OC, optical circulator; PD, photodetector; VNA, vector network analyzer.

polarization controller (PC1). After passing through the 1550-nm port of a wavelength division multiplexer (WDM), the light wave is launched into the sensor via a second PC (PC2) and an optical circulator (OC). The optical signal reflected by the FP resonators is converted to an electrical signal at a photodetector (PD). The pump light causes population inversion in the EYDF fiber. Due to the high absorption of the EYDF, a declining pump power and signal gain will be achieved along the pump direction. The gain and loss coefficients of FP1 and FP2 can thus be tuned by controlling the pump power. The phase-modulated optical light consisting of an optical carrier and two sidebands is applied to the sensor. Thanks to the PM-PM conversion, an MPF with two passbands corresponding to the two split wavelengths is implemented[22]. The frequency spacing of the two passbands is determined by the wavelength spacing of the two resonant wavelengths. By monitoring the spectral response of the MPF using a vector network analyzer (VNA), the bending curvature can be obtained. Thanks to the high resolution of the VNA, high bending curvature resolution can be realized.

Figure 6 shows the measured MPF spectral responses when the frequency splitting is increased from 0.5 to 1.51 GHz, corresponding to an increase in the curvature from 0.28 to 1.24 m^{-1} realized by adjusting MPP1 to apply a force to FP1. The minimal detectable frequency splitting is 0.50 GHz, corresponding to a curvature of 0.28 m^{-1}. The 3-dB bandwidth of the FP resonators is measured to be 298 MHz, which is approximately the minimum resolvable frequency splitting and thus determines the bending sensing resolution of the sensor. Assuming that the bending causes a resonance frequency shift of ε=298 MHz of FP2 in a non-EP case, we can calculate by Eq. (5) that the maximum sensitivity enhancement factor η=9.5 for the sensor with an EP-enabled nonlinear sensing response. Note that the 3-dB bandwidth of the FP resonators can be reduced by increasing the reflectivities of the FBGs during the fabrication by using a higher power UV

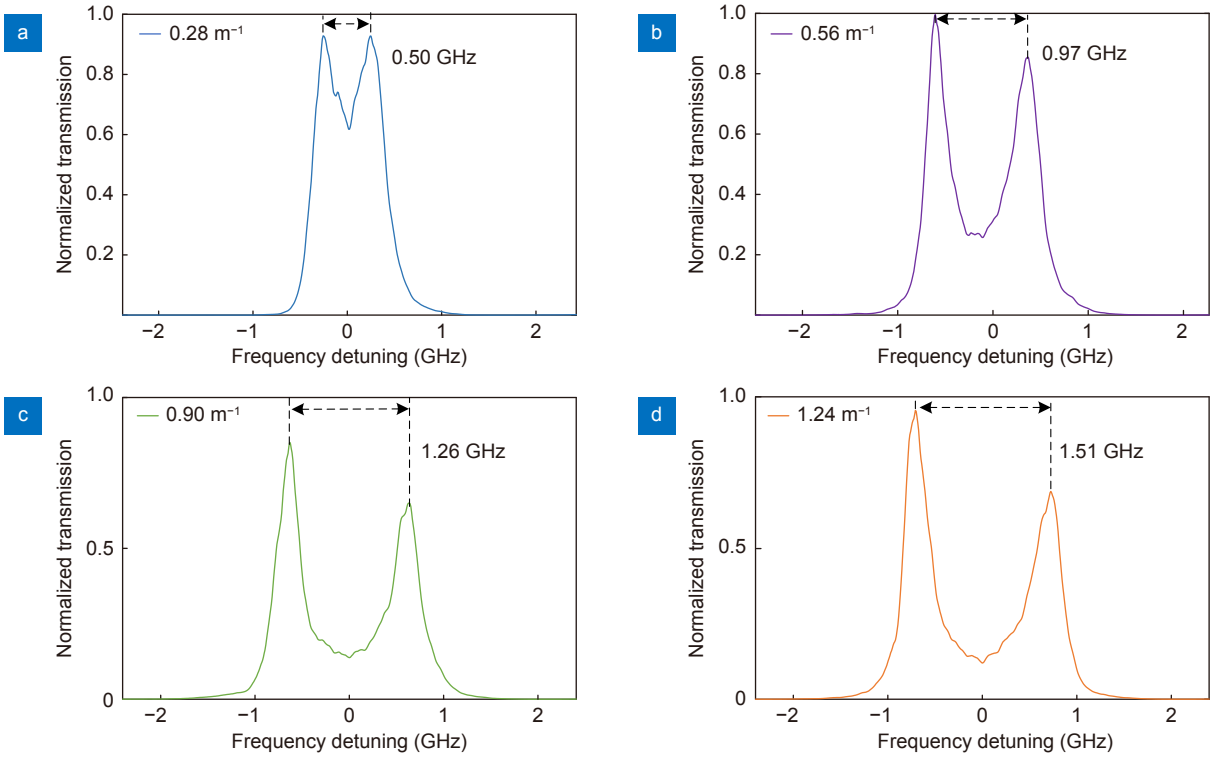

Fig. 6 | The spectral responses of the MPF when the curvature is increased from (**a**) 0.28, (**b**) 0.56, (**c**) 0.90 to (**d**) 1.24 m^{-1}.

laser to achieve higher refractive index modulation, which would result in the FP resonators to have higher Q factors, leading to a higher sensitivity enhancement and a higher curvature resolution.

The sensitivity enhancement based on the proposed EP-based fiber-optic bending sensor is studied. As can be seen from Fig. 7(a), the microwave frequency separation versus the fiber curvature change has a square-root relationship, which is confirmed in the logarithmic plot shown in the inset of Fig. 7(a) where the slope is 1/2. Note that the sensitivity is manifested as the slope of the sensing response curve in Fig. 7(a). Figure 7(b) depicts the measured sensitivity enhancement factor as a function of the curvature, which is obtained by calculating the ratio between the slope of the sensing response curve in Fig. 7(a) and that in the inset of Fig. 7(b). Note that the curve in the inset of Fig. 7(b) is obtained by measuring the resonance wavelength detuning between FP1 and FP2 as a function of the curvature for a non-EP-based condition. It shows a linear relationship, thus the sensitivity (the slope of the curve) is a constant. The sensitivity of the EP-based sensor with a nonlinear sensing response is greatly enhanced near the EP. From Fig. 7(b), we can observe a maximum enhancement in frequency splitting by a factor of 4 when the curvature is below 0.5 m^{-1}. If the resonance bandwidths of the FP resonators are further reduced, the enhancement can be higher[9,10,27], which can be done by optimizing the FBG parameters or by employing an active fiber with a higher doping concentration[28].

The stability of the proposed sensor is also studied. To do so, we allow the device to stay at a room temperature of 24 °C with ±2 °C with a fixed curvature of 0.56 m^{-1} for five hours, the eigenfrequency splitting is measured and the results show that the variations have a standard deviation of less than 1 MHz, corresponding to a curvature accuracy of 7.56×10^{-4} m^{-1}. The high stability of the sensor is owing to the relatively large reflection bandwidth of the FBGs of over 0.3 nm, in which only temperature variations in the order of 100 °C can lead to a significant change in the EP condition of $-\gamma = \kappa$.

Discussion and conclusion

The key challenge in making such a sensor is the fabrication of identical FP cavities on an optical fiber, especially when fabricating the three FBGs individually. The issue can be resolved by employing a customized mask in which three FBGs with the designed parameters are incorporated. The FP cavity length is then defined by the phase mask, which ensures high fabrication precision to the sub-nanometer scale and allows high repeatability and reproducibility. Such a grating fabrication process is suitable for large-scale mass production.

In conclusion, a fiber-optic bending sensor with EP-enhanced sensitivity based on PT-symmetric FP resonators was proposed and experimentally demonstrated. The resonance frequency splitting with a square-root dependence on the curvature perturbation strength around the EP was exploited to achieve high curvature sensing sensitivity. To interrogate the sensor at a higher speed and a higher resolution, the spectral response of the EP sensor was mapped to the microwave domain by implementing a dual passband MPF with the center frequencies of the two passbands corresponding to the two splitting wavelengths. Thus, high-accuracy measurement with sub-GHz resolution was achieved. The bending

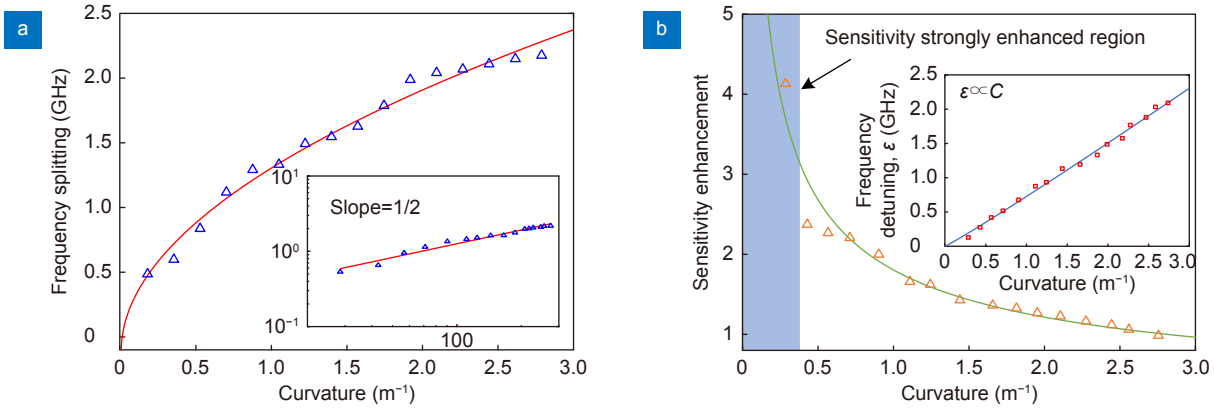

Fig. 7 | (**a**) Microwave frequency splitting as a function of the optical fiber curvature. Inset shows the results in a logarithmic scale. (**b**) Measured enhancement factor as a function of the optical fiber curvature. Inset shows the measured resonance frequency detuning between FP1 and FP2 as a function of the optical fiber curvature.

sensor has a curvature accuracy of 7.56×10^{-4} m^{-1} and a curvature sensitivity of 1.32 GHz/m^{-1} for a measurement range from 0.28 to 0.90 m^{-1}, which is more than 4 times higher than those without EP-enhanced sensitivity. The average sensitivity is 0.66 GHz/m^{-1} over the entire sensing range from 0.28 to 2.74 m^{-1} with a 3.78×10^{-7} m^{-1} measurement resolution.

References

1. Udd E. An overview of fiber-optic sensors. *Rev Sci Instrum* **66**, 4015–4030 (1995).
2. Kersey AD, Davis MA, Patrick HJ, LeBlanc M, Koo KP et al. Fiber grating sensors. *J Lightwave Technol* **15**, 1442–1463 (1997).
3. Wang Q, Liu Y. Review of optical fiber bending/curvature sensor. *Measurement* **130**, 161–176 (2018).
4. Wada D, Igawa H, Murayama H. Simultaneous distributed measurement of the strain and temperature for a four-point bending test using polarization-maintaining fiber Bragg grating interrogated by optical frequency domain reflectometry. *Measurement* **94**, 745–752 (2016).
5. Zheng D, Madrigal J, Barrera D, Sales S, Capmany J. Microwave photonic filtering for interrogating FBG-based multicore fiber curvature sensor. *IEEE Photonics Technol Lett* **29**, 1707–1710 (2017).
6. Zhang YS, Zhang WG, Chen L, Zhang YX, Wang S et al. Concave-lens-like long-period fiber grating bidirectional high-sensitivity bending sensor. *Opt Lett* **42**, 3892–3895 (2017).
7. Xiao DR, Wang GQ, Yu FH, Liu SQ, Xu WJ et al. Optical curvature sensor with high resolution based on in-line fiber Mach-Zehnder interferometer and microwave photonic filter. *Opt Express* **30**, 5402–5413 (2022).
8. Wiersig J. Enhancing the sensitivity of frequency and energy splitting detection by using exceptional points: application to microcavity sensors for single-particle detection. *Phys Rev Lett* **112**, 203901 (2014).
9. Chen WJ, Kaya Özdemir Ş, Zhao GM, Wiersig J, Yang L. Exceptional points enhance sensing in an optical microcavity. *Nature* **548**, 192–196 (2017).
10. Hodaei H, Hassan AU, Wittek S, Garcia-Gracia H, El-Ganainy R et al. Enhanced sensitivity at higher-order exceptional points. *Nature* **548**, 187–191 (2017).
11. Lai YH, Lu YK, Suh MG, Yuan ZQ, Vahala K. Observation of the exceptional-point-enhanced Sagnac effect. *Nature* **576**, 65–69 (2019).
12. Dong ZY, Li ZP, Yang FY, Qiu CW, Ho JS. Sensitive readout of implantable microsensors using a wireless system locked to an exceptional point. *Nat Electron* **2**, 335–342 (2019).
13. Yu S, Meng Y, Tang JS, Xu XY, Wang YT et al. Experimental investigation of quantum *PT*-enhanced sensor. *Phys Rev Lett* **125**, 240506 (2020).
14. Kononchuk R, Cai JZ, Ellis F, Thevamaran R, Kottos T. Exceptional-point-based accelerometers with enhanced signal-to-noise ratio. *Nature* **607**, 697–702 (2022).
15. Bender CM, Boettcher S. Real spectra in non-Hermitian Hamiltonians having *PT* symmetry. *Phys Rev Lett* **80**, 5243–5246 (1998).
16. Özdemir ŞK, Rotter S, Nori F, Yang L. Parity–time symmetry and exceptional points in photonics. *Nat Mater* **18**, 783–798 (2019).
17. Li Z, Zhang JJ, Zhi YY, Li LZ, Liao BL et al. All-fiber optical nonreciprocity based on parity-time-symmetric Fabry-Perot resonators. *Commun Phys* **5**, 332 (2022).
18. Li LZ, Cao Y, Zhi YY, Zhang JJ, Zou YT et al. Polarimetric parity-time symmetry in a photonic system. *Light Sci Appl* **9**, 169 (2020).
19. Zhang JJ, Li LZ, Wang GY, Feng XH, Guan BO et al. Parity-time symmetry in wavelength space within a single spatial resonator. *Nat Commun* **11**, 3217 (2020).
20. Wang HT, Guo J, Zhang JN, Zhou W, Wang YS et al. Sensing enhancement at an exceptional point in a nonreciprocal fiber ring cavity. *J Lightwave Technol* **38**, 2511–2515 (2020).
21. Liu XL, Wang HT, Zhang JN, Guo J, Wu X. Enhancement of sensitivity near exceptional point by constructing nonreciprocal fiber cavity assisted by isolator and erbium-doped fiber. *IEEE Sens J* **21**, 18823–18828 (2021).
22. Li WZ, Li M, Yao JP. A narrow-passband and frequency-tunable microwave photonic filter based on phase-modulation to intensity-modulation conversion using a phase-shifted fiber Bragg grating. *IEEE Trans Microwave Theory Tech* **60**, 1287–1296 (2012).
23. Yao JP. Microwave photonics for high-resolution and high-speed interrogation of fiber Bragg grating sensors. *Fiber Integr Opt* **34**, 204–216 (2015).
24. Deng H, Zhang WF, Yao JP. High-speed and high-resolution interrogation of a silicon photonic microdisk sensor based on microwave photonic filtering. *J Lightwave Technol* **36**, 4243–4249 (2018).
25. Hodaei H, Miri MA, Heinrich M, Christodoulides DN, Khajavikhan M. Parity-time–symmetric microring lasers. *Science* **346**, 975–978 (2014).
26. Zhao Y, Cai L, Li XG. Temperature-insensitive optical fiber curvature sensor based on SMF-MMF-TCSMF-MMF-SMF structure. *IEEE Trans Instrum Meas* **66**, 141–147 (2017).
27. Wiersig J. Prospects and fundamental limits in exceptional point-based sensing. *Nat Commun* **11**, 2454 (2020).
28. Boetti NG, Scarpignato GC, Lousteau J, Pugliese D, Bastard L et al. High concentration Yb-Er co-doped phosphate glass for optical fiber amplification. *J Opt* **17**, 065705 (2015).

Acknowledgements

This work was supported by the Guangdong Province Key Field R&D Program Project (2020B0101110002), National Key R&D Program of China (2021YFB2800804) and the National Natural Science Foundation of China (61905095, 62101214).

Author contributions

Z. Li, J. J. Zhang and J. P. Yao conceived the idea and wrote the paper; Z. Li conducted the theoretical simulations, device fabrication, and testing; J. X. Chen and L. Z. Li contributed to device fabrication and testing.

Competing interests

The authors declare no competing financial interests.